Exciton-exciton annihilation and saturation effect in TbF_3

M. F. Joubert, B. Jacquier, and R. Moncorgé
Equipe (No. 10) de Recherche du Centre National de la Recherche Scientifique, Université de Lyon I, F-69622 Villeurbanne, France
(Received 2 August 1982; revised manuscript received 31 January 1983)

Blue ($^5D_4 \rightarrow {}^7F_6$) as well as uv anti-Stokes ($^5D_3 \rightarrow {}^7F_6$) fluorescences are observed in TbF_3 at low temperature when the $^5D_4$ Stark components of the Tb^{3+} active ions are excited. In addition, when the $^5D_4$ exciton density is high enough, holes appear in the center of each excitation line of the visible emission, and in the corresponding absorption spectrum as well. Fluorescence dynamics and intensities are then studied for increasing pump powers. These properties are expressed as combinations of exciton-exciton annihilation and cross-relaxation processes. Saturation effects on both intrinsic and perturbed Tb^{3+} ions are discussed.

I. INTRODUCTION

In this paper we examine the effect of the optical pump power on the fluorescence properties of the nominally pure terbium fluoride TbF_3. The motivation of this study was to obtain a better knowledge of the dynamical processes responsible for the very efficient visible to uv energy conversion already observed[1] and the strong optical hole-burning effect, which is unusual in such a self-activated material.

Since photon fluxes of 10^{14}–10^{18} photons per cm^2 per pulse are easily attainable with the currently available short-pulsed lasers, a very high density of excitation can be obtained whenever an appreciable absorption cross section exists. When such a high density is produced, new optical phenomena, up conversion for example, may occur. In that case, the interpretations must be adapted to the correct nature of the entities which come into play in the various systems.

In strongly coupled organic solids,[2,3] the up-conversion process is usually ascribed to exciton-exciton annihilation. It results in a nonexponential exciton decay which depends nonlinearly on the excitation pump power. This effect has been observed also in manganese fluorides such as MnF_2,[4] $KMnF_3$,[5] and $CsMnF_3$.[6] The wavelike nature of the optical excitations does make sense in these materials since the coherence of the excitons could have been observed either directly, in organic compounds, from the triplet exciton line shape,[7,8] or indirectly, in transition-metal antiferromagnets, through its effect on the exciton diffusion.[9,10]

In rare-earth compounds such as $TbPO_4$ (Ref. 11) and TbF_3 (Ref. 12) where one measures fairly low macroscopic diffusion coefficients ($D \sim 10^{-10}$–10^{-9} $cm^2 s^{-1}$), the excitons could be better described by incoherent hopping excitations. This seems to be more accurate in rare-earth salts, as the $4f$ electrons involved in the optical transitions are shielded. In that case, the exciton-exciton annihilation process mentioned above might be interpreted as an up-conversion process between two coupled neighboring active ions. This would also result in a nonexponential decay depending nonlinearly on the excitation pump power.

However, it has been shown that a low diffusion coefficient does not necessarily eliminate the exciton picture.[6,13] Indeed, the existence of spectrally well-defined $\vec{k}$ excitons has been proved, for example, in the case of low-dimensional ferromagnets $Tb(OH)_3$ (Refs. 14 and 15) and $GdCl_3$ (Ref. 16) where non-negligible exciton dispersions of 0.4 and 1 cm^{-1}, respectively, have been reported.

Though it would be a significant issue, the questions of coherent versus hopping character for the excitons and the possible effect of the different nature of rare-earth excitons on annihilation will not be analyzed in this paper since this should not influence the result of our macroscopic measurements.

The electronic configuration of the Tb^{3+} ion is $4f^8$. Including spin-orbit coupling, the electronic ground state of the free ion is a ^7F_J ($J=0,1,\ldots,6$) multiplet and the first excited states are $^5D_4$ and $^5D_3$. The corresponding absorption bands (f-f transitions) lie at about 20 600 (Ref. 17) and 26 000 cm^{-1}, above which the spacing of the different J levels is reduced (<2000 cm^{-1}), and the strong absorption band, relative to the interconfigurational transition $4f^8 \rightarrow 4f^7$-$5d$ appears at $\sim 40\,000$ cm^{-1}. Within TbF_3—space group D_{2h}^{16}—the Tb^{3+} ions are situated in a crystal field of Cs symmetry.[18] Thus we expect the $(2J+1)$-fold degeneracy of the various free-ion terms listed above to be totally removed.

We have recently reported the fluorescence properties of TbF_3 at low temperatures.[19] The positions of the $^7F_6$ and $^5D_4$ Stark components needed in the following are indicated in Fig. 1. By using time-resolved techniques we have pointed out the coexistence of bulk active Tb^{3+} ions and fluorescing traps, Tb^{3+} ions (perturbed by neighboring impurities or defects) which have their energy levels depressed with respect to the former. In particular, in order to explain the dynamical properties of the blue fluorescence ($^5D_4 \rightarrow {}^7F_6$) observed at 4.4 K, a diffusion model involving both shallow traps and deeper traps has been proposed for the overall exciton (unperturbed or intrinsic bulk ions) to trap energy-transfer processes in this material: Under low optical pumping conditions ($E_{exc} \simeq 30$ μJ per pulse unfocused), the blue intrinsic fluorescence decay is made of two exponential components, the shortest one giving rise to the true $^5D_4$ exciton lifetime $\tau_2 = 179$ μs, the longest one arising from the thermal depopulation of definite shallow traps.

In this study we analyze the conditions under which the $^5D_3$ anti-Stokes fluorescence appears and the processes which affect the $^5D_4$ exciton dynamics using intense selective dye-laser excitation. Details are given about the sa-

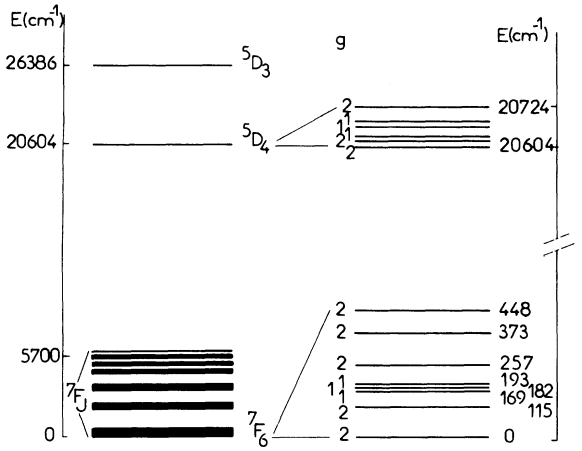

FIG. 1. Energy levels of Tb^{3+} ions in TbF_3 with the Stark components of the $^5D_4$ and $^7F_6$ multiplets. $g=1,2$ indicates singlet or doublet component, respectively.

turation effects observed in the excitation and absorption spectra as well.

In Sec. II we describe the material studied and the experimental equipment used here more specifically. Section III is devoted to a description of the data resulting from this investigation. At the end, a discussion is developed in terms of exciton-exciton annihilation and cross-relaxation mechanisms.

II. MATERIAL AND EXPERIMENTAL EQUIPMENT

The TbF_3 single crystal was grown in Hughes Laboratory using the Czochralski method. This transparent sample is of good optical quality. However, even in a pure material, the presence of impurities and defects cannot be avoided. The chemical analysis has shown that the chief rare-earth contaminants are Pr^{3+} and Gd^{3+} ions at concentrations of about 30 ppm each ($\sim 10^{18}$ ions/cm^3 in TbF_3). Three samples of different thickness, 0.35, 1.14, and 3 mm, with optically polished faces, have been used in our spectroscopic measurements at low temperature.

The magnetization[20] and neutron-diffraction data[21] indicate that orthorhombic TbF_3 orders ferromagnetically below 3.95 K. Since new energy-transfer mechanisms, due to the competition of the magnetic interactions, for example, could be involved in this temperature domain, all the experiments which are described in the following have been reported at higher temperatures, in particular, at $T=4.4$ K.

Selective excitation has been accomplished using a frequency-tripled Quantel model 481 infrared yttrium aluminum garnet (YAG):Nd^{3+} laser (pulse width = 10 ns, repetition rate 10 Hz, and peak power 12 Mw at 3550 Å) followed by a three-stage amplifier dye laser (pulse width = 10 ns, linewidth ~ 0.2 cm^{-1}). With the use of a Intertechnique model IN90 multichannel analyzer, the fluorescence data have been recorded and processed over 256 channels with a maximum resolution of 2 μs per channel. The fluorescence decays at shorter times have been recorded over 2048 channels on a computer-interfaced Biomation transient recorder with a resolution of 10 ns per channel.

To observe the absorption spectra under saturating conditions, two dye-laser beams have been used. The details of this experiment will be presented later in Sec. III B with the corresponding results.

III. EXPERIMENTAL RESULTS

As we mentioned before, a very recent study[19] allowed us to point out the efficiency of energy transfer from intrinsic Tb^{3+} ions to Tb^{3+} fluorescing traps in pure TbF_3, in perfect agreement with a model of fast exciton diffusion and trapping. All the experiments reported in this previous paper were carried out at low pump intensities, typically of the order of $E=30$ μJ per pulse (~ 3 kW peak power), giving rise to initial $^5D_4$ exciton densities $N_2(0)$ of $(1.3\pm0.5)\times10^{17}$ cm^{-3}. The laser was partially focused onto an aperture area $A\simeq 3.6\times10^{-3}$ cm^2, and the absolute value of $N_2(0)$ was obtained using the following equation:

$$N_2(0)=\frac{N(1-e^{-\alpha x})}{Ax},$$

where N was the number of photons per excitation pulse, $\alpha=7.2$ cm^{-1} was the absorption coefficient, and $x=0.035$ cm was the sample thickness. The precision of the measurement of E, x, and especially A led $N_2(0)$ to an uncertainty better than a factor of 2.

As the laser power, i.e., the $^5D_4$ exciton density, was increased, two important effects were observed: (A) the appearance of an uv anti-Stokes fluorescence coming from the upper excited state $^5D_3$; (B) at even higher laser intensities, the appearance of optical holes in the excitation spectra of both the intrinsic and trap $^5D_4\rightarrow{}^7F_6$ fluorescences.

A. uv anti-Stokes fluorescence

The uv anti-Stokes fluorescence spectrum obtained at 4.4 K by exciting in the lowest component of the $^5D_4$ manifold located at 4852.1 Å (20 604 cm^{-1}, see Fig. 1) is presented in Fig. 2 and summarized in Table I. Since the relative positions of the seven main lines coincide exactly with the crystal-field energy splitting of the $^7F_6$ ground multiplet (see Fig. 1), and since the emission line located at 3788.75 Å (26 386.43 cm^{-1}) is resonant with the absorption line corresponding to the lowest $^7F_6\rightarrow{}^5D_3$ transition, the uv fluorescence is attributed to the $^5D_3\rightarrow{}^7F_6$ transition. In addition, the whole excitation spectrum of the most intense uv fluorescence line compares very well with the excitation spectrum of the blue fluorescence originating from the $^5D_4$ level shown in Fig. 3(a) which, in turn, closely corresponds to the $^7F_6\rightarrow{}^5D_4$ absorption bands of the crystal.[19]

The emission line at 3855.2 Å remains the most intense line, while the relative intensity of the others changes with temperature in the range 4.4—50 K. We now focus attention on the power dependence of the anti-Stokes fluorescence. The integrated emission intensity of the 3855.2-Å anti-Stokes fluorescence depends first, quadratically, on the excitation pump power for $^5D_4$ exciton densities up to 10^{18} cm^{-3} and then, linearly. This is shown in Fig. 4 where the horizontal axis of the main graph is $N_2(0)$,

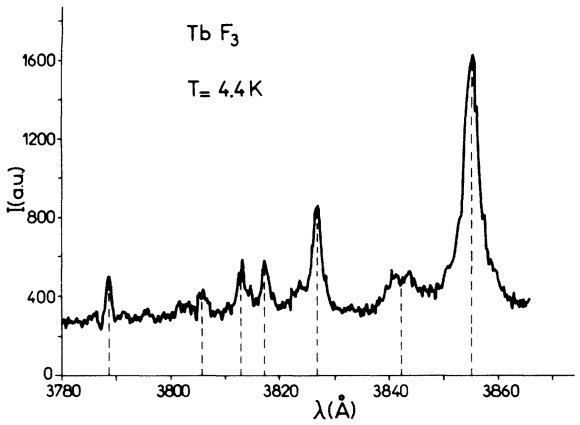

FIG. 2. uv anti-Stokes fluorescence spectrum of Tb^{3+} ions under 20 604-cm^{-1} (4852.1-Å) excitation.

while that of the inset is $N_2^2(0)$, to emphasize the quadratic behavior at low excitation powers. Within each of these two regimes, the dynamics proceed as follows.

1. "Low" $^5D_4$ exciton densities

At 4.4 K the time evolution of the uv anti-Stokes fluorescence presents a short rise-time behavior up to ~ 0.3 μs, and then an exponential decrease with a time constant $\tau_3 = 89$ μs [see Fig. 5(b)], half the value of the $^5D_4$ exciton lifetime of 179 μs, which is obtained under low pumping conditions. On the other hand, when the $^5D_3$ level is directly pumped by the frequency-tripled radiation of the YAG:Nd^{3+} laser at 3550 Å, the $^5D_3$ uv fluorescence signal is then very weak and decays exponentially with the time constant $\tau_3' = 70$ ns.

This lifetime discrepancy clearly shows the origins of the $^5D_3$ fluorescence in each case: The uv anti-Stokes emission results from a cooperative effect involving two $^5D_4$ excitons, while the 70-ns time constant and the weak efficiency of the directly pumped $^5D_3 \rightarrow {}^7F_6$ emission indicates the role of the strong cross-relaxation process which depletes the $^5D_3$ in favor of the $^5D_4$ level because of the matching energies $^5D_3$-$^5D_4$ and $^7F_6$-$^7F_1$ for two neighboring Tb^{3+} ions (see Figs. 1 and 5).

Subsequently, at sufficiently high $^5D_4$ exciton densities, when the uv anti-Stokes fluorescence can be observed, the

TABLE I. Position of the anti-Stokes emission lines corresponding to the $^5D_3 \rightarrow {}^7F_6$ transition.

Position	
λ (Å)	ν (cm^{-1})
3788.5	26 386
3806.0	26 267
3813.3	26 216
3817.5	26 188
3826.9	26 123.5
3842.5	26 017
3855.2	25 932

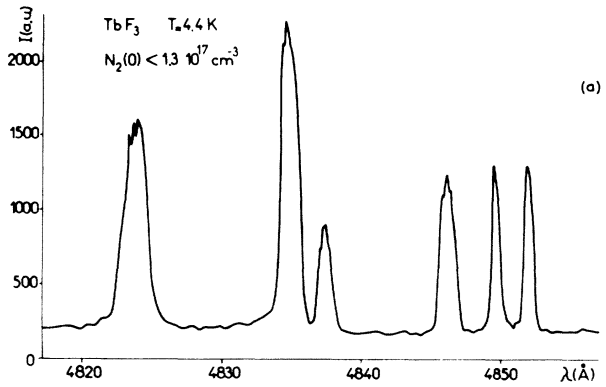

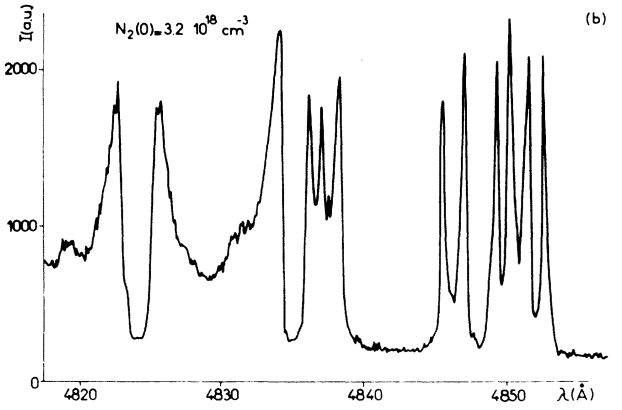

FIG. 3. Excitation spectra of the blue fluorescence line located at 4863.3 Å (20 560 cm^{-1}) with (a) $N_2(0) = 1.28 \times 10^{17}$ cm^{-3} and (b) $N_2(0) = 3.2 \times 10^{18}$ cm^{-3}.

$^5D_4$ fluorescence decay exhibits a nonexponential behavior as shown in Fig. 6. These exciton densities favor an exciton-exciton annihilation process in which two coupled $^5D_4$ excitons relax at short times to promote an excitation at twice their energies, thus populating the $^5D_3$ upper lev-

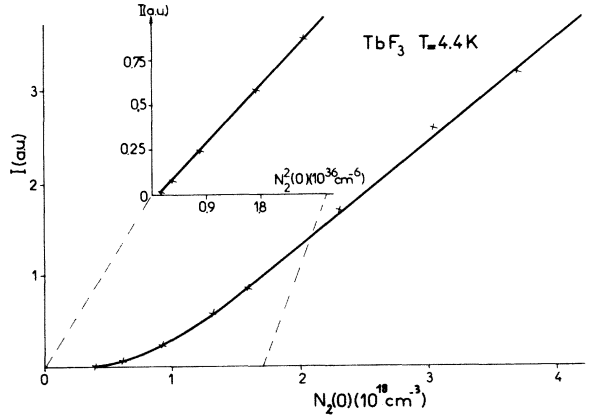

FIG. 4. Intensity of the uv anti-Stokes fluorescence line (3855.2 Å) vs the initial $^5D_4$ exciton density at 4.4 K.

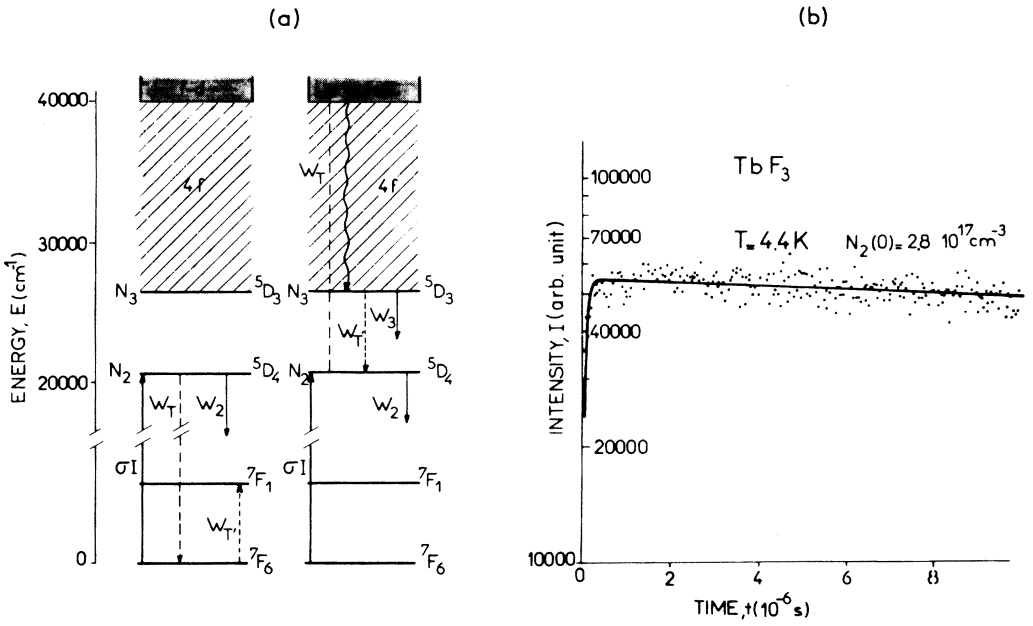

FIG. 5. (a) Model for the uv anti-Stokes fluorescence. (b) Semilog plot of the experimental (· · · ·) and calculated (——) decays for this anti-Stokes fluorescence.

el. At longer times, when the $^5D_4$ exciton density is low, the situation goes back asymptotically to a single-ion process and the $^5D_4$ fluorescence decay becomes exponential again.

2. *"High" $^5D_4$ exciton densities*

When the anti-Stokes emission depends linearly on the $^5D_4$ exciton density (right-hand side of Fig. 4), the $^5D_3$ fluorescence decay is no longer exponential: An additional process must be involved, this being enlightened by the experimental observations presented in the next section.

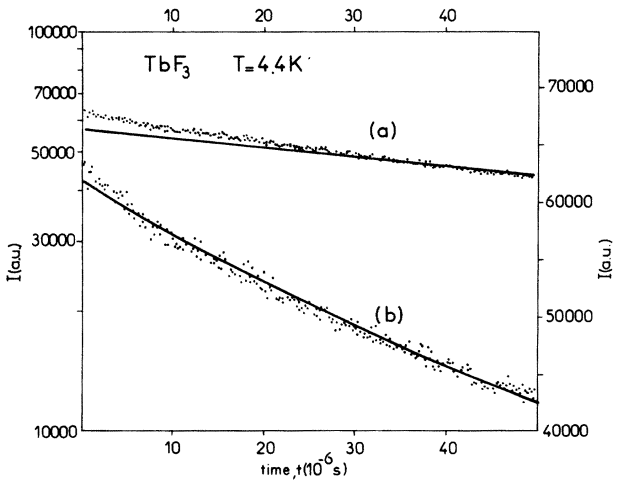

FIG. 6. Decay for the intrinsic blue fluorescence line located at 4852.8 Å (20 600 cm^{-1}) when the excitation pulse creates an initial $^5D_4$ exciton density of 1.3×10^{18} cm^{-3}. (a) Left-hand scale: semilog plot of the experimental data (· · · ·) and calculated exponential decay (——) with a τ time constant of 179 μs. (b) Right-hand scale: linear plot of the experimental data (· · · ·) and calculated decay (——) using Eq. (11).

B. Hole-burning experiments

Looking at either the intrinsic or trap blue fluorescence, we record the $^5D_4$ excitation spectra under increasing pump powers. First, the excitation lines get about the same intensity, and then holes appear at their center and become more and more pronounced [see Fig. 3(b)]. This effect decreases the whole visible fluorescence efficiency. In particular, at $T=4.4$ K, when the trap fluorescence is the most intense, a complete extinction of it can be achieved: The depth of the holes reaches the noise level of the photomultiplier. We have noted that the position of each hole does not change with the observed emission line. The excitation spectra of the intrinsic fluorescence do not experience such an important effect. Either at higher pump powers or higher temperatures, where the intrinsic fluorescence dominates, holes never exceed 30% of the total intensity of each of the excitation lines. In order to avoid any complexity which could come with excitation data from dynamical effects other than saturation, we perform the following hole-burning absorption experiment. Two dye-laser beams are used: a wide band saturating beam ($\delta=3$ cm^{-1}, $E=0.3$ mJ/pulse), centered at the maximum of the absorption band and focused onto the crystal, and a narrow band ($\delta=0.2$ cm^{-1}) probe beam at the right angle of the latter, focused onto the region of the sample already illuminated. The two dye lasers are pumped by the same YAG:Nd^{3+} laser source mentioned in Sec. II to eliminate any jitter effects. The two beams enter the crystal perpendicularly because it is cut at 90°; incidentally, the detection of the probe light transmitted by the sample is easier. The signal is analyzed by a filtered S20 photomul-

tiplier and fed into a PAR boxcar averager with a gate width of 20 ns. The saturating beam is fixed at $\lambda=4823.95$ Å (20 724 cm^{-1}), which is the position of the higher-energy component of the $^7F_6 \rightarrow {}^5D_4$ absorption transition, the one presenting the deepest hole in the excitation spectra under high pump powers. The 3-cm^{-1} bandwidth of this laser beam allows a quasicomplete overlapping with absorption line. Figure 7 shows the profile of the absorption line when the saturating beam is on [Fig. 7(a)] and off [Fig. 7(b)]. The hole corresponds to an increase of the intensity of the light transmitted by the crystal at the center of the line, thus indicating a beginning of saturation of the associated absorbing level for an exciton density of about 2.3×10^{18} cm^{-3}.

IV. INTERPRETATION

In a previous study[19] we had evaluated in TbF_3 an average diffusion coefficient $D\sim8.6\times10^{-10}$ cm^2s^{-1} which established, using a nearest-neighbor hopping model, that the optical excitation was spread over many intrinsic Tb^{3+} ions before reaching any Tb^{3+} fluorescing traps. The resulting hopping time $t_H\sim2\times10^{-7}$ s might be sufficiently short to allow the present experimental observations to be interpreted in terms of excitons.

However, because, in most cases, intraband relaxations are fast compared with the time scale of our measurements, we will develop in the following an incoherent-type formalism in which the wave-vector-dependent exciton populations will be replaced by thermal averages. On the basis of the rate equations governing the uv anti-Stokes fluorescence, we examine first the excited-state populations as a function of the optical pump power. Then it is shown how the saturation effect can be taken into account within this formalism.

A. uv anti-Stokes fluorescence

When intrinsic Tb^{3+} ions are excited at $\lambda=3550$ Å by the frequency-tripled YAG:Nd^{3+} laser, i.e., into the higher absorption bands, the excited ions rapidly relax first to the $^5D_3$ level then to the lowest excited $^5D_4$. In particular, the last step is favored, in TbF_3, by the good energy matching between $^5D_3$-$^5D_4$ ($\Delta E\sim5725\pm60$ cm^{-1}) and $^7F_6$-$^7F_1$ ($\Delta E\sim5703\pm97$ cm^{-1}), thus by the very efficient cross-relaxation process which depletes the $^5D_3$ excited state to the advantage of the $^5D_4$. This results, in our experiments, in the observed very short decay time $\tau_3'=70$ ns and the poor quantum efficiency of the $^5D_3\rightarrow{}^7F_6$ fluorescence. This is inferred when looking at the response of a very dilute material such as $Y_3Al_5O_{12}$: 0.09% Tb^{3+}; in this case the cross-relaxation process is much less efficient and a time constant of 1.45 ms is measured,[22] in good agreement with the value which is expected for a $4f^8$ intraconfigurational transition.

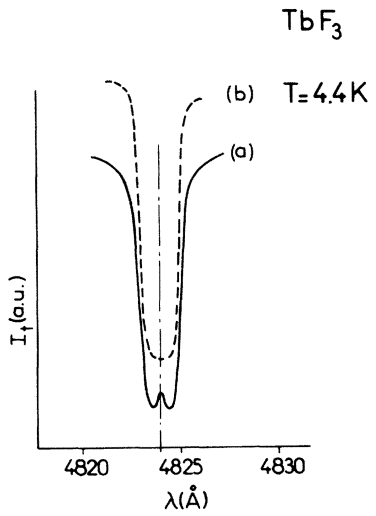

FIG. 7. Absorption line at 4823.95 Å (20 724 cm^{-1}) when saturating beam is (a) on and (b) off.

1. Fluorescence dynamics

The model proposed to interpret the anti-Stokes fluorescence is based on both the exciton-exciton annihilation and the cross-relaxation process mentioned above [Fig. 5(a)]. When the intrinsic Tb^{3+} ions are excited into the lower-energy component of the $^5D_4$ multiplet, i.e., at $\lambda=4852.1$ Å (20 604 cm^{-1}), the $^5D_4$ exciton density may be sufficient to allow exciton-exciton interaction. Two $^5D_4$ excitons then annihilate to create an excitation (a single exciton located on one of the interacting ions for weak coupling or a biexciton as in a pair process for strong coupling) at about twice their energy, i.e., at $\sim41\,208$ cm^{-1}, an energy which corresponds to the absorption tail of the excited configuration $4f^7$-$5d$. After a rapid relaxation (phonon-assisted process) to the $^5D_3$ level, the $^5D_3$ and the $^5D_4$ populations noted N_3 and N_2 evolve according to the following rate equations:

$$\frac{dN_2}{dt}=N_1\sigma I-W_2N_2-W_{EC}N_2^2+W_{CR}N_3N_1\ , \tag{1}$$

$$\frac{dN_3}{dt}=\tfrac{1}{2}W_{EC}N_2^2-W_{CR}N_3N_1-W_3N_3\ , \tag{2}$$

where N_1 is the population in the ground state, σ is the absorption cross section, I is the laser-beam intensity, W_2 and W_3 are the decay rates of levels $^5D_4$ and $^5D_3$ without cross relaxation, and W_{EC} and W_{CR} are the transfer rates by exciton collision and cross relaxation, respectively. Owing to the high efficiency of the cross-relaxation process in TbF_3, we make first the following assumption:

$$W_{CR}N_1N_3\gg W_3N_3\ . \tag{3}$$

Using then the approximation $N_1=N=$density of Tb^{3+} absorbing centers, we write

$$W_3N_3+W_{CR}N_3N_1\simeq W_{CR}N_1N_3\simeq W_3'N_3\ , \tag{4}$$

where W_3' measures the decay rate of the directly pumped $^5D_3\rightarrow{}^7F_6$ fluorescence, i.e.,

$$W_3'^{-1}=\tau_3'=70\ ,$$

measured in ns. We get then the simplified equations

$$\frac{dN_2}{dt}=N_1\sigma I-W_2N_2-W_{EC}N_2^2+W_3'N_3\ , \tag{5}$$

$$\frac{dN_3}{dt}=\tfrac{1}{2}W_{EC}N_2^2-W_3'N_3\ . \tag{6}$$

a. Very low optical pumping regime [$N_2(0) < 10^{18}$ cm^{-3}]. Under such conditions, the $^5D_4 \rightarrow {}^7F_6$ exciton fluorescence decays exponentially over 2 orders of magnitude at times $t \lesssim 400$ μs. Since fluorescence is found to be linearly dependent on the excitation pump power, i.e., on the initial exciton density $N_2(0)$, the time evolution of the $^5D_4$ exciton population takes the form

$$N_2(t) = N_2(0) e^{-W_2 t} . \tag{7}$$

By substituting this in Eq. (6), the $^5D_3$ exciton population transforms similar to

$$N_3(t) = \frac{W_{EC} N_2^2(0)}{2(W_3' - 2W_2)} (e^{-2W_2 T} - e^{-W_3' t}) . \tag{8}$$

Decay curves for both the visible and the uv anti-Stokes fluorescences were fitted successfully with relations (7) and (8), respectively. In particular [see Fig. 5(b)], the value obtained for the anti-Stokes fluorescence time constant τ_3 is in perfect agreement with half the value of the visible fluorescence lifetime τ_2, i.e.,

$$\tau_3 = (2W_2)^{-1} = 89 ,$$

$$\tau_2 = W_2^{-1} = 179 ,$$

measured in μs. In addition, the time $t_M = 0.5$ μs, at which the anti-Stokes fluorescence intensity reaches its maximum, correlates well with

$$t_M = \frac{1}{W_3' - 2W_2} \ln \frac{W_3'}{2W_2} , \tag{9}$$

an expression directly obtainable from relations (7) and (8) in which we have inserted the values of W_2 and W_3' resulting from the fits to the data. The rise behavior for the anti-Stokes fluorescence is adequately given by the measured decay rate W_3' of the directly pumped $^5D_3 \rightarrow {}^7F_6$ fluorescence. Within this formalism, we note that, under very low optical pump powers, neither the visible nor the uv fluorescence time-evolution experiences any effect from the exciton-exciton collision parameter W_{EC}.

b. Higher pumping regime [$10^{18} < N_2(0) < 2.10^{18}$ cm^{-3}]. At higher excitation powers, the $^5D_4 \rightarrow {}^7F_6$ fluorescence decay is no longer exponential. It shortens at short times after the laser pulse and the emission intensity increases nonlinearly with the excitation. This is attributed to an increasing $^5D_4$ exciton density which makes the collision processes more and more probable. Consequently, the nonlinear term in Eq. (5) becomes non-negligible and we must solve Eqs. (5) and (6) entirely. However, as was done in the past,[11] we shall assume that the condition $dN_3/dt = 0$ is fulfilled so that, after the laser pulse ($I = 0$), Eq. (5) transforms as

$$\frac{dN_2}{dt} = -W_2 N_2 - \tfrac{1}{2} W_{EC} N_2^2 . \tag{10}$$

We are left with a Bernouilli differential equation, the solution of which is given by

$$N_2(t) = \left[-\frac{W_{EC}}{2W_2} + \left[\frac{1}{N_2(0)} + \frac{W_{EC}}{2W_2} \right] e^{W_2 t} \right]^{-1} . \tag{11}$$

As shown in Fig. 6(b), this new time evolution agrees fairly well with the $^5D_4 \rightarrow {}^7F_6$ fluorescence decay which is experimentally observed. The fit to the data leads to the exciton-exciton annihilation coefficient (measured in $cm^3 s^{-1}$)

$$W_{EC} \simeq 3.5 \times 10^{-15} .$$

In addition, the complete numerical resolution of Eqs. (5) and (6) without assuming $dN_3/dt = 0$ and including the above calculated collision rate W_{EC}, gives a decay curve which is strictly identical to the fitting curve. When varying the value of W_{EC}, the agreement either with the fitting points or the experimental data is not as good, thus proving the validity of our primary assumption, i.e., $dN_3/dt = 0$.

With the use of the framework of the exciton random walk, the collision parameter W_{EC} is expressed as follows:

$$W_{EC} = 8\pi D_0 \langle R \rangle . \tag{12}$$

When the average interaction radius $\langle R \rangle$ is set equal to the mean separation between neighboring Tb^{3+} ions, i.e., $\langle R \rangle = 4$ Å, expression (12) allows us to calculate a maximum diffusion coefficient $D_0 \simeq 3 \times 10^{-9}$ $cm^2 s^{-1}$, a limit which corresponds well to the value (8.6×10^{-10} $cm^2 s^{-1}$) that we had previously calculated using a fast-diffusion model for exciton to trap energy transfers.[19] The discrepancy between these two estimations of D_0 might come from the existence of microscopic exciton domains.[13] The diffusion coefficient which is obtained through the exciton collision parameter, that is, from short-time experimental data, would correspond to the effective diffusion of the excitons within these microscopic regions. The average diffusion coefficient that we obtained from the exciton to trap energy-transfer data, that is, at longer times after the laser pulse, would correspond to a macroscopic diffusion including diffusion within and between different excitonic regions.

2. Intensity measurements

The anti-Stokes fluorescence intensity has been measured for initial $^5D_4$ exciton densities between 0.3×10^{18} and 4×10^{18} cm^{-3}, a domain in which $N_1 \simeq N$ holds, to a good approximation, since we are dealing with a great number of Tb^{3+} ions in TbF_3. The theoretical description of the anti-Stokes fluorescence intensity versus the exciton density is enumerated now as follows.

a. Very low optical pumping regime [$N_2(0) < 10^{18}$ cm^{-3}]. The $^5D_4$ and $^5D_3$ exciton populations are given by relations (7) and (8) where $N_2(0)$ is proportional to the laser-beam intensity I. The intensities I_2 and I_3 of the visible and uv anti-Stokes fluorescences are written

$$I_2 = h\nu_{12} W_r \langle N_2 \rangle , \tag{13}$$

$$I_3 = h\nu_{13} W_{3r} \langle N_3 \rangle , \tag{14}$$

where $h\nu_{12}$ and $h\nu_{13}$ are the energies of the respective emitted photons, W_r and W_{3r} stand for the radiative emission probabilities of levels $^5D_4$ and $^5D_3$, $\langle N_2 \rangle$ and $\langle N_3 \rangle$ are the time-averaged exciton populations. Since $\langle N_2 \rangle$ is proportional to $N_2(0)$,[23] I_2 depends linearly on $N_2(0)$, e.g., on the excitation pump power I. On the other hand, using expression (8), I_3 is found to be quadratically dependent on the laser intensity. Both results agree with the experimental observation.

b. High pumping regime $[2\times10^{18}<N_2(0)<4\times10^{18}$ $cm^{-3}]$. The excitation spectra showed us that the intrinsic visible fluorescence did not increase linearly any longer with the excitation density; it was increasing more slowly. Moreover, we noted the appearance of holes, indicating then a diminution of the visible fluorescence quantum yield. A complete extinction of the fluorescence emitted by the perturbed Tb^{3+} ions was observed. These experimental considerations lead us to neglect the term W_2N_2 in Eq. (5) when the excitation density is sufficiently high. The integration of Eqs. (5) and (6) over the time scale θ ($\theta=100$ ms) between two successive laser pulses gives then

$$N_1\sigma I\frac{\Delta\theta}{\theta}=\tfrac{1}{2}W_{\mathrm{EC}}\langle N_2^2\rangle\ , \tag{15}$$

$$\tfrac{1}{2}W_{\mathrm{EC}}\langle N_2^2\rangle=W_3'\langle N_3\rangle\ , \tag{16}$$

where $\Delta\theta$ represents the pulse duration ($\Delta\theta\simeq10$ ns).

These expressions mean that for high pumping powers, the anti-Stokes emission intensity which is proportional to $\langle N_3\rangle$ varies linearly with the laser-beam intensity I in strict agreement with the observation. This result verifies *a posteriori* the validity of the approximation made above in Eqs. (5) and (6) on the relative efficiency of terms $W_{\mathrm{EC}}N_2^2$ and W_2N_2.

B. Saturation effects

At very low pump powers, the crystal emits a strong green fluorescence. At very high pump powers, when the laser excitation is situated at the center of an absorption line of the $^7F_6\rightarrow{}^5D_4$ transition, this visible fluorescence disappears. This is confirmed by looking at the excitation spectra of the trap fluorescence [Fig. 5(b)]: 90% of the total visible emission consists of this trap fluorescence and the holes in the corresponding excitation spectra quickly reach the noise level of our photomultiplier.

Before showing that these effects are completely consistent with a saturation process, the possibility that they are due to radiative energy transfer or laser local heating has to be considered. When radiative energy transfer occurs, the exciton decay must be dependent on the position of the excitation in the crystal. Moreover, only the $^5D_4\rightarrow{}^7F_6$ blue fluorescence would be modified. Instead, no change of the exciton decay is observed by varying the physical position of the excitation with respect to the observation, and the fluorescence extinction effect concerns the whole visible emission. Laser local heating as a source of fluorescence quenching is also ruled out, since a change in the excitation spectra induced by temperature would correspond to a change of the exciton decay in its whole time domain, which is not observed. The extinction of the very intense trap fluorescence at 4863.3 Å, for example (see Sec. III B), is definitively attributed to a saturation process.

Within an oversimplified two-level system, where level 1 stands for the ground state and level 2 for the excited state, the populations N_1 and N_2 of these levels satisfy the following equation[24]:

$$\frac{d\Delta N}{dt}=-\Delta N\left[\frac{1}{\tau_0}+\frac{2\sigma I}{\hbar\omega}\right]+\frac{N_T}{\tau_0}\ , \tag{17}$$

in which $\Delta N=N_1-N_2$, N_T is the total population of the system, τ_0 is the lifetime of level 2, σ is the absorption cross section of transition $1\rightarrow2$, and I and ω are the intensity and the frequency of the excitation source, respectively. At steady state, the solution of Eq. (17) is written

$$\Delta N=\frac{N_T}{1+I/I_s}\ , \tag{18}$$

with $I_s=\hbar\omega/2\sigma\tau_0$. I_s is the saturation intensity at which $\Delta N=N_T/2$.

When one examines the effect of saturation on homogeneously broadened absorption lines by performing the two-beam experiment detailed before, one gets the same formal result, and the absorption coefficient $\alpha(\omega')$, which is measured by the probe beam at the frequency ω', transforms as

$$\alpha(\omega')=\frac{\alpha_0(\omega')}{1+I_\omega/I_s}\ , \tag{19}$$

where $\alpha_0(\omega')$ is the absorption coefficient when the saturating wave at the frequency ω is absent. If the intensity I_ω of this saturating wave is increased, the absorption coefficient $\alpha(\omega')$ is reduced by a factor which does not depend on ω', and no hole can be observed in the absorption line shape.

In the case of inhomogeneously broadened lines, the saturation phenomenon becomes more complicated since one deals with a superposition of homogeneous systems. Qualitatively, the intensity I_ω will interact essentially with those ions whose resonant frequency is in the neighborhood of ω, and the absorption coefficient $\alpha(\omega')$ given by the probe beam at the frequency ω' equals $\alpha_0(\omega')$ reduced by a factor which depends on $\omega-\omega'$.[25] This reduction factor becomes more pronounced for $\omega'=\omega$, and a hole appears in the absorption line at the frequency ω of the saturating wave.

In TbF_3, owing to the crystal-field inhomogeneities throughout the lattice, one deals with inhomogeneously broadened transitions, and holes can be potentially observed in the spectra when one satisfies the saturation requirements. The saturation of the $^5D_4$ excited state can be explained as follows: As we mentioned above, at $T=4.4$ K, 90% of the absorbed energy is transferred to the Tb^{3+} fluorescing traps. Thus with a $^5D_4$ exciton density of 3.2×10^{18} cm^{-3}, a density at which the excitation spectrum of Fig. 3(b) was recorded and the extinction was almost complete, the density of the excited fluorescing traps is 2.9×10^{18} cm^{-3}. The comparison of this number with the overall concentration of fluorescing traps, i.e., 1.2×10^{19} cm^{-3}, then allows us to determine $\Delta N=6.2\times10^{18}$ cm^{-3} for the system of perturbed Tb^{3+} ions. Consequently, the saturation conditions for the existence of holes in the excitation spectra of the fluorescing traps are clearly verified since for the system of perturbed ions $N_T=1.2\times10^{19}$ cm^{-3} and $\Delta N>N_T/2=6\times10^{18}$ cm^{-3}.

As we noted in the experimental data obtained at $T=4.4$ K, holes were also observed in the excitation spectra of the intrinsic fluorescence and only very weakly in the absorption spectrum in the presence of a saturating beam (see Fig. 7). This much weaker effect is attributed to the large concentration of the intrinsic absorbing centers with respect to the traps. The excitation holes are ex-

plained as follows: Back transfers from shallow traps were shown[19] previously to give a non-negligible contribution (few percent) to the $^5D_4$ exciton decay in the long-time limit. We then assert that the holes which are effectively observed in the intrinsic excitation spectra arise from the saturation of these shallow traps. Indeed, for identical pumping conditions, the intensity ratio of the excitation holes for the intrinsic and trap fluorescences compares adequately with the ratio of the intensities, which can be inferred to result from the $^5D_4$ exciton decay coming from the contribution of shallow traps in the long-time limit and from the contribution of the overall exciton to trap energy transfers at shorter times.

If the hole effect in the intrinsic excitation spectra can be interpreted in a similar manner as above, the beginning of saturation which is observed in absorption still remains a matter of discussion. A mechanism such as two-photon stepwise absorption could be involved. This would be inferred by the behavior of the anti-Stokes fluorescence decay. Indeed, at high pump powers, this experimental fluorescence decay no longer exhibits its characteristic rise-time behavior; it starts instead with a nonzero intensity, indicating then the possibility of a direct pumping process. Experiments are in progress to clarify this point.

V. CONCLUSION

In a previous paper[19] we were interested in studying the processes which affect the energy transfer and $^5D_4$ exciton decay in the nominally pure TbF_3 system. This paper was devoted more specifically to the investigation of the process responsible for the strong uv anti-Stokes fluorescence and the optical holes which appear under high pumping conditions.

The $^5D_3 \rightarrow {}^7F_6$ anti-Stokes fluorescence is interpreted in terms of exciton-exciton annihilation. For sufficiently low pump powers, however, the $^5D_4$ exciton decay remains exponential, and the anti-Stokes fluorescence presents a short rise-time behavior which is related to the fast relaxation process between levels $^5D_3$ and $^5D_4$. In agreement with the theoretical predictions also, the $^5D_4 \rightarrow {}^7F_6$ visible fluorescence increases linearly with the excitation intensity, while the $^5D_3 \rightarrow {}^7F_6$ anti-Stokes emission increases quadratically with it. At sufficiently high pump powers, the $^5D_4$ exciton decay shortens at short times; the resulting decay curve yields the exciton-exciton collision parameter $W_{EC} \simeq 3.5 \times 10^{-15}$ cm^3 s^{-1}. At even higher pump powers, the uv anti-Stokes fluorescence increases linearly with the excitation intensity, and holes appear in the excitation spectra in agreement with saturation effects on the Tb^{3+} perturbed ions (traps). However, the existence of holes in the absorption spectra relative to the Tb^{3+} intrinsic system (bulk ions) is only qualitatively explained. A better description could be given by taking into account both the complicated level structure of the Tb^{3+} ions and the dynamical properties (exciton-exciton annihilation, cross relaxation) which characterize these ions in TbF_3. It is clear that further work is needed on this very interesting material.

ACKNOWLEDGMENTS

The authors are grateful to M. Blanchard, A. Lagriffoul, and C. Madej for their technical assistance, and to G. Boulon, J. C. Gâcon, and A. Koningstein for helpful discussions. Thanks are also expressed to Mr. M. Robinson (Hughes Laboratory) for having kindly provided us with the single crystal used here.

[1]M. F. Joubert, B. Jacquier, G. Boulon, and R. Moncorgé, in Minutes of the Third Conference of Dynamical Processes in the Excited States of Ions and Molecules in Solids, Third Dynamical Processes Conference, Regensburg, 1981 [Bull. Am. Phys. Soc. 27, 65 (1982)].

[2]R. G. Kepler, J. C. Caris, P. Avakian, and E. Abramson, Phys. Rev. Lett. 10, 400 (1963).

[3]A. Bergman, M. Levine, and J. Jortner, Phys. Rev. Lett. 18, 593 (1967).

[4]B. A. Wilson, J. Hegarty, and W. M. Yen, Phys. Rev. Lett. 41, 268 (1978).

[5]E. Strauss, W. J. Maniscalco, W. M. Yen, U. C. Keffner, and V. Gerhardt, Phys. Rev. Lett. 44, 824 (1980).

[6]R. Moncorgé, B. Jacquier, M. Blanchard, and C. Madej, J. Phys. (Paris) 43, 85 (1982).

[7]B. M. Shelby, A. H. Zewail, and C. B. Harris, J. Chem. Phys. 64, 3192 (1976).

[8]C. B. Harris, Chem. Phys. Lett. 52, 5 (1977).

[9]R. M. MacFarlane and A. C. Luntz, Phys. Rev. Lett. 31, 832 (1973).

[10]K. Ueda and Y. Tanabe, J. Phys. Soc. Jpn. 48, 1137 (1980).

[11]P. C. Diggle, K. A. Gehring, and R. M. MacFarlane, Solid State Commun. 18, 391 (1976).

[12]M. F. Joubert, Ph.D. thesis, University of Lyon, 1982 (unpublished).

[13]H. T. Chen and R. S. Meltzer, Phys. Rev. Lett. 44, 599 (1980).

[14]R. L. Cone and R. S. Meltzer, J. Chem. Phys. 62, 3573 (1975).

[15]R. S. Meltzer, Solid State Commun. 20, 553 (1976).

[16]R. S. Meltzer and H. W. Moos, Phys. Rev. B 6, 264 (1972).

[17]D. C. Krupka and H. J. Guggenheim, J. Chem. Phys. 51, 4006 (1969).

[18]A. Zalkin and D. H. Templeton, J. Am. Chem. Soc. 75, 2453 (1953).

[19]M. F. Joubert, B. Jacquier, R. Moncorgé, and G. Boulon, J. Phys. (Paris) 43, 893 (1982).

[20]L. Holmes, H. J. Guggenheim, and G. W. Hull, Solid State Commun. 8, 2005 (1970).

[21]M. Piotrowski and A. Murasik, Phys. Status Solidi A 60, K195 (1980).

[22]D. J. Robbins, B. Cockayne, B. Lent, and J. L. Glasper, Solid State Commun. 20, 673 (1976).

[23]This can be shown by the calculation of the integration of $N_2(t)$ over the time scale θ between two successive laser pulses.

[24]O. Svelto, *Principles of Lasers* (Plenum, New York, 1976), p. 56.

[25]A. Yariv, *Quantum Electronics*, 2nd ed. (Wiley, New York, 1975), p. 171.

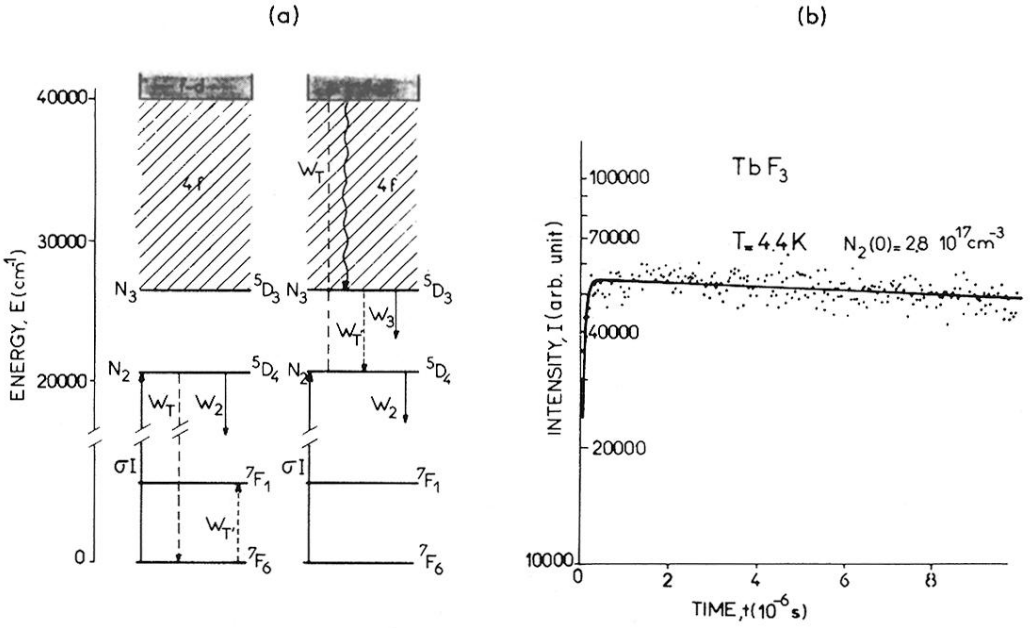

FIG. 5. (a) Model for the uv anti-Stokes fluorescence. (b) Semilog plot of the experimental (· · · ·) and calculated (——) decays for this anti-Stokes fluorescence.